# Dalton Transactions

Accepted Manuscript



This is an *Accepted Manuscript*, which has been through the Royal Society of Chemistry peer review process and has been accepted for publication.

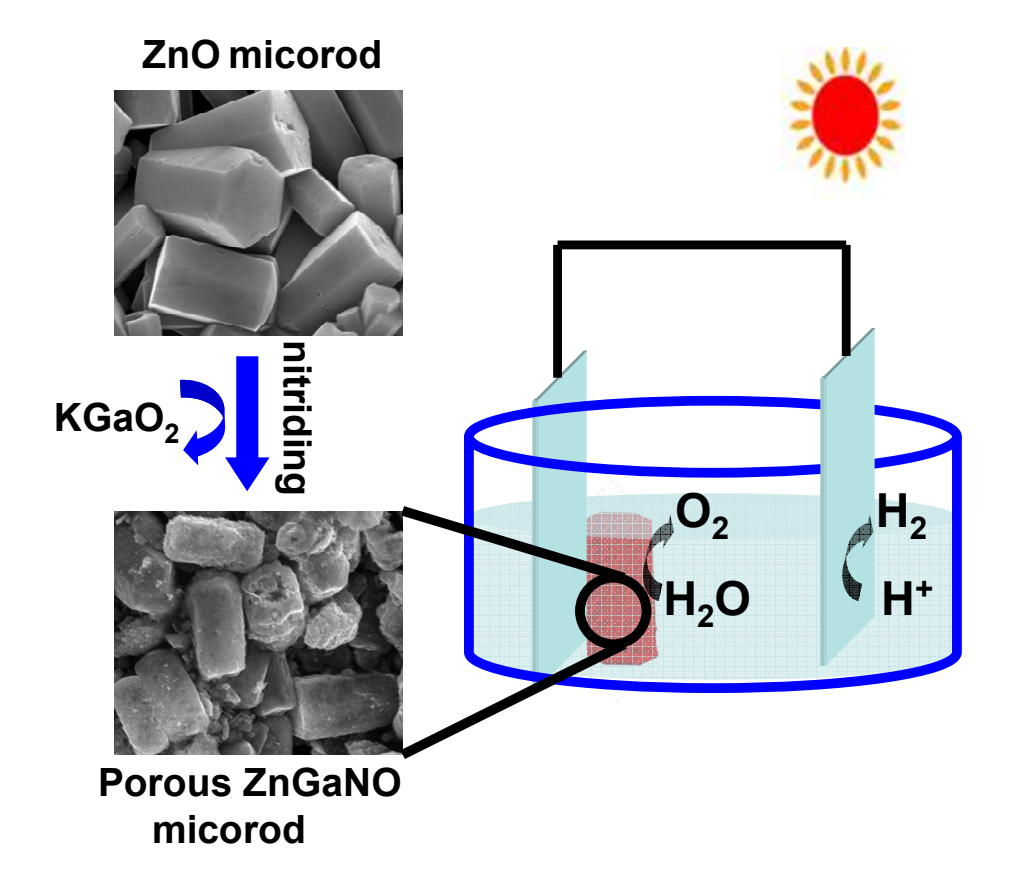
Accepted Manuscripts are published online shortly after acceptance, before technical editing, formatting and proof reading. Using this free service, authors can make their results available to the community, in citable form, before we publish the edited article. We will replace this Accepted Manuscript with the edited and formatted Advance Article as soon as it is available.

You can find more information about *Accepted Manuscripts* in the **Information for Authors**.

Please note that technical editing may introduce minor changes to the text and/or graphics, which may alter content. The journal's standard <u>Terms & Conditions</u> and the <u>Ethical guidelines</u> still apply. In no event shall the Royal Society of Chemistry be held responsible for any errors or omissions in this *Accepted Manuscript* or any consequences arising from the use of any information it contains.



# **Graphical abstract**



## Dalton Transactions

**RSCPublishing** 

### **COMMUNICATION**

# A porous ZnGaNO photoanode for efficient water oxidation modified by Co-based electrocatalyst

Cite this: DOI: 10.1039/xoxxooooox

S.C. $Yan^{a,b^*}$  and Z.G. $Zou^{a,b,c}$ 

Received ooth January 2012, Accepted ooth January 2012

DOI: 10.1039/x0xx00000x

www.rsc.org/

Porous ZnGaNO microrods were synthesized by a single crystal internal decomposition route, exhibited the high performance in photoelectrochemical water splitting due to the high specific area and short charge transfer distance by microstructure.

#### 1. Introduction

Oxynitrides are important functional materials, with applications in many fields such as the photocatalysis, luminescence, functional ceramics and inorganic pigment. In particular, for the photocatalysis, oxynitrides, which usually have moderate band gap and good photostability, were considered to be the promising materials to drive the artificial photosynthesis reaction. To apply this technique, the high-activity photocatalyst was expected. Recently, much interest has been focused on research into the synthesis of nanostructured semiconductor crystals with high surface area and small particle size to improve the efficiency in photocatalytic water splitting. Typically, nanostructure performance enhancements have been observed with low electrical conductivity of Fe<sub>2</sub>O<sub>3</sub> 9,10 and BiVO<sub>4</sub>, 11,12 owing to the increased contact area between electrolyte and surface of semiconductor and a shortening of charge transport pathways from material interior to the surface.

Oxynitrides were generally synthesized via direct reactions of oxides with NH<sub>3</sub>, usually at high temperature. The crystallite size is not restricted by the low sinterability of oxynitrides because the oxides itself usually sinter readily at the reaction temperature. Therefore, little progress has been made in the synthesis of nanostructured oxynitrides. A limited number of porous oxynitrides, such as the SiO<sub>x</sub>N<sub>y</sub> and NbSiON, 13,14 were prepared by nitriding the high-temperature stable Si-containing porous oxides. Nitriding the mesoporous ZnGa<sub>2</sub>O<sub>4</sub>, the mesoporous ZnGaNO solid solution was obtained. 15,16 Such a synthetic route can be named 'reactive templating' route. In this synthetic route, the high-temperature stable oxides with the specific nanostructures were used as a reactive template. The nanostructure of oxide precursors is maintained in the generated oxynitrides after high temperature nitriding. Usually, the high surface area of oxide nanoparticles was needed to improve their reactivity with NH<sub>3</sub>, reducing reaction temperature for avoiding the

collapse of nanostructures. In recent years, another route that involves a pseudomorphous and topotactic phase transformation was developed to synthesize the porous oxynitrides, such as the porous TaON nanoparticles <sup>17</sup> and porous LaTiO<sub>2</sub>N <sup>18</sup> single crystal particles. In this route, the porous structure formed during the nitriding reaction, owing to the change in crystal volume during the phase transformation from the oxide to oxynitride. In these reported routes, the oxynitrides with nanostructure can be obtained by using the single oxide as starting reagent. A challenge to achieve the nanoscale design of oxynitrides prepared by using the precursors containing more than one type of oxide is still remained, because it is difficult to avoid the collapse of nanostructures occurring in the phase transformation among oxide precursors and also not easy to balance the low thermal stability of oxide nanoparticles and the requirement of high nitriding temperature to form oxynitrides.

Here, we for the first time developed a single-crystal oxide reactive template route to prepare the porous zinc gallium oxynitride (ZnGaNO) microrods. In this route, the micrometer oxides, hexagonal single crystal ZnO microrods, can be used as the raw material, which react with another oxide, KGaO<sub>2</sub>, to form porous ZnGaNO in the ZnO microrods during nitriding. The profile of ZnO precursor was kept in the final product by assembling the ZnGaNO nanocrystals. Such a hierarchical architecture is significantly beneficial to obtain the high performance in photoelectrochemical water splitting due to the enhanced light use efficiency, increased electrode-electrolyte contact area and short charge transport pathways. Loading the Co-based hydroxide on the surface of ZnGaNO photoelectrode as an electrocatalyst, a record photocurrent for the ZnGaNO material was achieved under AM 1.5 solar illumination.

#### 2. Experimental details

*Material preparation:* A starting reagent, KGaO<sub>2</sub> powder, was synthesized by heating a stoichiometric mixture of K<sub>2</sub>CO<sub>3</sub> and Ga<sub>2</sub>O<sub>3</sub> at 900 °C for 12 h. To prepare ZnO microrods, 1.26g of aqueous ammonia was added into 200 mL of Zn(NO<sub>3</sub>)<sub>2</sub>·6H<sub>2</sub>O (0.001mol) aqueous solution. After magnetically stirred for 20 min at room temperature, the mixing solution was heated in water bath at

COMMUNICATION

90 °C for 4 h. The production was washed with de-ionized water, centrifuged and dried at 60 °C for 2 h. The as-prepared ZnO microrods (0.01mol) was added into 5mL of KGaO $_2$  (0.01mol) colloidal solution, magnetically stirred and dried for 1h at 70 °C. The as-obtained KGaO $_2$  colloid coated ZnO microrods were put into an alundum boat and followed by nitriding it into ZnGaNO solid solution using a tubular furnace with an inner diameter of 50 mm at 780 °C for 5 h with an NH $_3$  flowing rate of 250 mL min $^{-1}$ .

Sample characterization: Crystal phases of these samples were determined using an X-ray diffractometer (XRD, Rigaku Ültima  $\Box$ , Japan) operated at 40 kV and 40 mA using Cu Ka radiation. The diffuse reflectance spectra were recorded using a UV-Vis spectrophotometer (UV-2500, Shimadzu Co., Japan) and transformed to the absorption spectra according to the Kubelka-Munk relationship. The morphology was observed by using a transmission electron microscope (TEM, FEI Tecnai G2 F30 S-Twin, USA) and a field-emission scanning electron microscopy (FE-SEM, Nova NanoSEM 230, FEI). Nitrogen absorption-adsorption isotherms were measured at 77 K on a Micromeritics ASAP 2000 volumetric adsorption analyzer. Before the measurements, the samples were pretreated at 200 °C for 2h under flowing N<sub>2</sub> gas for clearing the surface. The BET specific surface areas were calculated using adsorption data acquired at a relative pressure (P/P<sub>0</sub>) range of 0.05-0.15. The pore size distribution curves were calculated from the analysis of the adsorption branch of the isotherm using the Barrett-Joyner-Halenda (BJH) algorithm.

Fabrication of ZnGaNO photoanodes: ZnGaNO photoanodes were fabricated using electrophoretic deposition (EPD) method followed by necking treatment. Typically, iodine (5 mg) and ZnGaNO (20 mg) powders were dispersed in acetone (25 mL) with the assistance of sonication to obtain the ZnGaNO powder suspension for EPD. The EPD process was conducted between two parallel FTO electrodes with the distance of 1 cm under 20 V of bias for 3 min. The coated area of the ZnGaNO film was ca. 1 cm×1cm. The electrodes were dried in air, and then dropped with TiCl<sub>4</sub> methanol solution (50 mM, 30µL). Finally, the dropped electrodes were heated at 350 °C for 30 min. The deposition of CoGa<sub>2</sub>O<sub>4</sub> water oxidation catalyst onto the ZnGaNO photoanodes was carried out by an impregnation method. The colloidal CoGa<sub>2</sub>O<sub>4</sub> solution was firstly prepared by the addition of NaGaO2 into an aqueous solution containing Zn<sup>2+</sup> ions. The as-prepared CoGa<sub>2</sub>O<sub>4</sub> colloidal solution (10mM, 10µL) was dropped on the surface of ZnGaNO photoelectrode by a pipette. Finally, CoGa<sub>2</sub>O<sub>4</sub> on the ZnGaNO electrodes were calcined at 300 °C for 10 min in air to form a highquality interface connection between CoGa<sub>2</sub>O<sub>4</sub> and ZnGaNO.

**PEC measurements:** PEC water-splitting properties of the hierarchical ZnGaNO microrod photoelectrodes were measured with the three-electrode configuration using a saturated calomel electrode (SCE) as reference electrode and a Pt wire counter electrode. An aqueous solution of 1M NaOH was used as the electrolyte. The measured potential versus SCE was converted to the reversible hydrogen electrode (RHE) scale according to the Nernst equation ( $E_{RHE}=E_{SCE}+0.059$  pH+0.241). The photoelectrodes were illuminated with AM 1.5G-simulated sunlight at 100mWcm<sup>-2</sup> from a Newport Sol3A Class AAA simulator. Current-potential curves were measured at a scan rate of 30mVs<sup>-1</sup> from negative to positive.

#### 3. Results and discussions

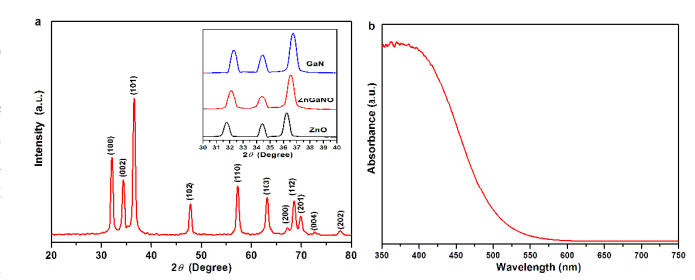


**Fig. 1** XRD pattern and optical properties of ZnGaNO microrods. a) XRD pattern. Inset shows the (100), (002) and (101) diffraction peaks for ZnO, ZnGaNO and GaN for comparison. b) UV-Vis absorption spectrum.

X-ray powder diffraction (XRD) was used to identify the crystal structure of as-prepared ZnGaNO. As shown in Fig. 1a, the ZnGaNO exhibits single-phase diffraction patterns indicative of the wurtzite structure similar to the ZnO precursor. The inset in Fig.1a shows a careful observation on the (100), (002) and (101) diffraction peaks of the ZnGaNO, along with GaN and ZnO data for comparison. The diffraction peak positions of the ZnGaON located between in those of GaN and ZnO. The cell constants of ZnGaNO are calculated according to the XRD data to be a=b=0.322 nm and c=0.520 nm, which are larger and smaller than those of GaN (a=b=0.319nm,c=0.519nm)<sup>19</sup> and ZnO (a =b=0.325nm, c=0.521nm)<sup>20</sup>, energy dispersive Xrespectively. The ray spectrometer analysis indicated that the composition of ZnGaNO solid solution is Zn<sub>0.17</sub>Ga<sub>0.3</sub>N<sub>0.3</sub>O<sub>0.24</sub> (Fig. S1 see ESI†). These data support a standpoint that the ZnGaNO is a solid solution of ZnO and GaN. The optical band gap of the ZnGaNO is obtained from its light absorption spectrum to be 2.38 eV (Fig. 1b), which is smaller than neither ZnO (3.2eV) nor GaN (3.4 eV), further confirming that the ZnGaNO is a solid solution of ZnO and GaN. 21

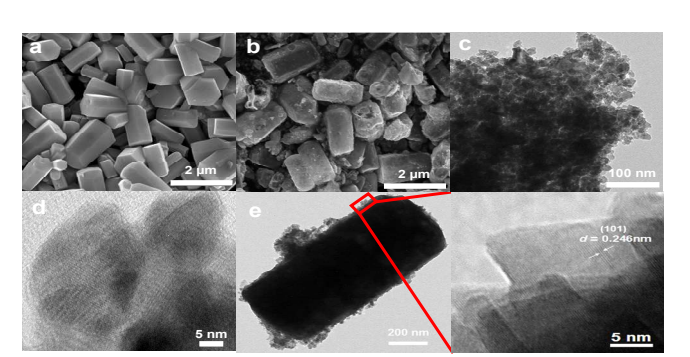


**Fig. 2** SEM and TEM images. a) SEM image of ZnO single crystal microrods. b) SEM image of porous ZnGaNO microrods. c) TEM image shows the porous structure of ZnGaNO microrods. d) High-resolution TEM shows the porous structure resulting from the accumulation of nanocrystals. e) TEM image for observing the ZnGaNO nanocrystal growth after heating the KGaO<sub>2</sub> coated ZnO microrod at 780°C for 1h. Inset shows the high-resolution TEM of crystal lattice.

The scanning electron microscopy (SEM) image in **Fig. 2a** and **b** reveals that the crystallographic properties of the ZnO microrods and ZnGaNO microrods with hierarchical architecture. The hexagonal ZnO single crystal microrods grew along the *c-axis* [001] with the exposed six (1 $\overline{10}$ ) equivalent facets parallel to *c-axis*. The diameter and length of single crystal ZnO measured from Fig.2a were  $\sim$ 0.5-1 and  $\sim$ 2-3 $\mu$ m, respectively. After nitriding the KGaO<sub>2</sub> colloid coated

ZnO microrods, ZnGaNO (Fig.2b) microrods with the hexagonal profile of ZnO precursor formed. TEM observation revealed that the ZnGaNO microrods possess a porous structure (Fig.2c). The nitrogen adsorption-desorption isotherms of as-prepared ZnGaNO further show that the isotherms are typical porous materials (Fig. S2 see ESI†). The pore diameter calculated from the nitrogen adsorption isotherm by the Barrett-Joyner-Halenda (BJH) method was 7.7 nm and the specific surface area calculated from the linear region of the Brunauer-Emmett-Teller (BET) plot ranging from P/P<sub>0</sub> = 0.05 to  $P/P_0 = 0.15$  was 47.2 m<sup>2</sup> g<sup>-1</sup>, which is about 3 times higher than 16.4 m<sup>2</sup> g<sup>-1</sup> for the ZnO microrods precursor. A high-resolution TEM (HR-TEM) image of the mesostructure revealed that the porous structure resulted from the aggregation of the nanocrystals with a particle size of 10-20 nm (Fig. 2d).

**Journal Name** 

Different with the previous strategy to the formation of pore in oxynitrides that uses the single oxide precursor by pseudomorphous and topotactic phase transformation or a porous reactive template, 15in our case, the porous ZnGaNO microrods were formed by nitriding the KGaO2 colloid coated ZnO single crystal microrods. The time-dependent observation was carried out for understanding the formation of the porous ZnGaNO microrods. At the initial stage of nitriding reaction, the ZnGaNO nanocrystals with the dominant (101) facet formed on the (110) surface of ZnO microrods (Fig. 2e). This phase transformation process will yield about 9% of volume shrinkage due to the GaN with a small cell volume incorporating into the ZnO. Therefore, the formation of pore can be attributed to the volume shrinkage during the nitriding reaction. As illustrated in Fig. S3 in ESI, it seems reasonable to speculate that the KGaO<sub>2</sub> colloid coating on the surface of ZnO microrods can flow through the porous ZnGaNO layer by seeping and continually reacts with ZnO to form the ZnGaNO nanocrystals. Indeed, the SEM observations and energy-dispersive spectrometry (EDS) analysis confirmed that the hydrosoluble KGaO<sub>2</sub> keeps the quasi-liquid state during the nitriding (Fig. S3 and S4 see ESI†), owing to the H<sub>2</sub>O formation from the nitriding reaction of the oxide. The hexagonal profile of ZnO microrods could be maintained in the generated ZnGaNO after nitriding, probably because the moderate reaction rate due to the same crystal structure between reagent ZnO and product ZnGaNO solid solution. The porous structure forming by aggregation of nanocrystals, which can compensate for the volume change by tuning the pore size, would be beneficial for maintaining the hexagonal framework of ZnO during nitriding reaction.

To investigate the photoelectrochemical properties of the hierarchical ZnGaNO porous microrods, the as-prepared ZnGaNO powders were coated as electrodes on fluorine-doped tin oxide (FTO) by an electrophoretic deposition technique. Under AM 1.5 G simulated sunlight (100 mW cm<sup>-2</sup>) irradiation, the ZnGaNO photoelectrode in 1M NaOH electrolyte exhibits a photocurrent of 10 μA cm<sup>-2</sup> at 1.23 V vs. RHE, which is about an order of magnitude higher than the reported ZnGaNO bulk particle electrode (Fig. S5 see ESI†).22 The photoluminescence (PL) analysis indicated that a PL peak at 650nm can be attributed to the defects formed in the ZnGaNO, as demonstrated in the ZnO.<sup>23, 24</sup> The PL peak intensity of the porous ZnGaNO microrods synthesized by nitriding reaction at 780 °C for 5h is about 10 times lower than the reported ZnGaNO bulk particle prepared by high-temparature nitriding for a prolonged time (850°C, 15h) (Fig. S6 see ESI†).<sup>22</sup> The high reaction temperature probably induced the formation of crystal defects such as the Zn or O vacancies due to the reducing atmosphere, which decreased the photoelectrochemical activity. In addition, the specific surface area of porous ZnGaNO microrods (40.7m<sup>2</sup>g<sup>-1</sup>) is about 6 times higher than that of the ZnGaNO bulk particles (8 m<sup>2</sup>g<sup>-1</sup>)

prepared by nitriding of ZnO and Ga<sub>2</sub>O<sub>3</sub>. <sup>22</sup> The porous structure in the ZnGaNO microrod inducing the high specific surface area is much beneficial to achieve the higher photoelectrochemical performance, as well demonstrated in mesoporous TiO2 single crystal.<sup>25</sup> Therefore, the improved photocurrent for the porous ZnGaNO microrod photoanode can be attributed to the low defect density and the porous structure increasing electrode-electrolyte contact area and shorting charge transport pathways. Indeed, to destroy the porous structure of ZnGaNO microrods into a dispersed nanocrystals by mechanically milling will lead to a decreased performance(**Fig. S7 see ESI**†). However, if compared to the other oxynitrides such as LaTiO<sub>2</sub>N, <sup>18</sup> such low photocurrent for porous ZnGaNO electrode is not satisfied.

Modifying the electrode surface with an appropriate oxygen evolution electrocatalyst is an efficient route for improving the separation and injection of charge carrier and lowering the overpotential.<sup>26</sup> Many Co-based materials, such as Co(OH)<sub>x</sub>, Co<sub>3</sub>O<sub>4</sub> and Co-Pi, were developed as the oxygen-evolution electrocatalyst, due to the low cost and high performance. For the Co-containing electrocatalysts, it is a challenge to construct a stable cobalt ion ligand environment for obtaining the stable and efficient catalytic performance. CoGa<sub>2</sub>O<sub>4</sub> is not a stable compound in the strong basic solution due to Ga leaching. Here we try to use porous CoGa<sub>2</sub>O<sub>4</sub> with high specific surface area of 253.2 m<sup>2</sup>g- (synthesis and characterization, Fig. S8-10 see ESI†) as a precursor to obtain Cobased electrocatalyst with the high catalytic performance. After Ga leaching, the porous structure of CoGa<sub>2</sub>O<sub>4</sub> is expected to be inherited in the Co-based oxide products. To confirm the proposed route, the as-prepared porous CoG<sub>a2</sub>O<sub>4</sub> powders were coated as electrodes on fluorine-doped tin oxide (FTO) by an electrophoretic deposition technique. The current-time scan was performed at 1.72 V vs RHE on CoGa<sub>2</sub>O<sub>4</sub> electrode in 1M NaOH electrolyte for 10h for obtaining a stable Co-based catalyst. A high-resolution TEM (HR-TEM) image (Fig. S11 see ESI†) of the crystal lattice can clearly identify that there are two types of lattice spacing in the Co-based electrocatalyst. The lattice spacing of 0.237 and 0.438 nm can be identified to the (011) plane of Co(OH)<sub>2</sub> and the (003) plane of CoOOH, respectively. Such a mixture of Co(OH)<sub>2</sub> and CoOOH was formed by Ga leaching and OH ions incorporating, meaning that the as-prepared Co-based mixture would be ions-impregnating catalyst with excellent mass transport due to the porous structure.

Here, the mixture of Co(OH)2 and CoOOH prepared by using CoGa<sub>2</sub>O<sub>4</sub> as a precursor, was used as an electrocatalyst to improve the catalytic performance of ZnGaNO electrode. As shown in Fig. 3a, the oxidation peaks A<sub>1</sub> and A<sub>2</sub> in cyclic voltammograms for the mixture of Co(OH)2 and CoOOH can be attributed to the oxidation of Co<sup>2+</sup> to Co<sup>3+</sup> and Co<sup>3+</sup> to Co<sup>4+</sup> species, respectively.<sup>27</sup> The appreciable catalytic current is observed beginning at overpotential  $\eta$ =0.28 V, and a current density of 10 mAcm<sup>-2</sup> requires  $\eta$ =0.47 V which is much lower than the existing Co-containing catalysts such as Co-Pi. 28 After loading Co-based electrocatalyst on the ZnGaNO photoelectrode surface, the dark current was much lower than the photocurrent (Fig. S12 see ESI†). The best photocurrent for porous ZnGaNO microrod photoanode with Co(OH)<sub>2</sub> and CoOOH was achieved to be 1mA cm<sup>-2</sup> at 1.23 V vs. RHE, about two orders of magnitude higher than the bare ZnGaNO microrod photoanode. For comparison, the Co<sub>3</sub>O<sub>4</sub> was also used as electrocatalyst to modify the ZnGaNO microrod photoanode by using the reported method.<sup>29</sup> The photocurrent for the Co<sub>3</sub>O<sub>4</sub> loaded ZnGaNO photoanode reached to 0.12mA cm<sup>-2</sup> at 1.23 V vs. RHE, much lower than the mixture of Co(OH)<sub>2</sub> and CoOOH modified ZnGaNO photoanode. It has been well demonstrated that the photocatalytic performance of ZnGaNO was dependent strongly on the use of cocatalysts to create the

COMMUNICATION

microrod.

suitable reaction sites.<sup>30</sup> In our case, the improved performance of the Co(OH)2+CoOOH loaded ZnGaNO photoanode probably resulted from that the low excess potential was required to oxidize Co<sup>2+</sup> to much higher valence state. In addition, SEM observation on the Co-based electrocatalyst loaded ZnGaNO photoelectrode after high pressure gas purging indicated that a high-quality interface formed between Co-based electrocatalyst and ZnGaNO (Fig. 4a), which is beneficial to decreasing the interface barrier for charge carrier transfer.In addition, the photoanode of the ZnGaNO bulk particles prepared at 850°C, <sup>22</sup> also exhibited the performance improvement in photoelectrochemical water splitting before and after Co-based electrocatalyst modification (Fig.S5 and Fig.3b). Photoactivity of the Co(OH)2+CoOOH loaded ZnGaNO bulk particle photoanode is much lower than that of Co(OH)<sub>2</sub>+CoOOH modified porous ZnGaNO microrod photoanode. This further confirmed that the porous structure and low defect density greatly contributed the performance enhancement of the porous ZnGaNO

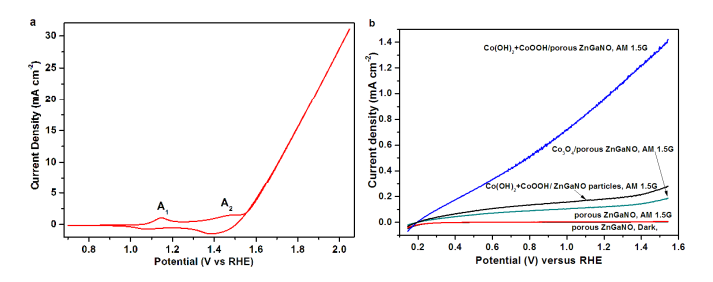


**Fig. 3** a) Cyclic voltammogram of as-prepared Co-based electrocatalyst obtained by the current-time scan on CoGa<sub>2</sub>O<sub>4</sub> electrode at 1.72 V vs RHE in 1M NaOH electrolyte for 10h. b) Current-potential curves for ZnGaNO microrod photoanode, Co(OH)<sub>2</sub>+CoOOH/ZnGaNO microrod photoanode, Co(OH)<sub>2</sub>+CoOOH/ZnGaNO particles photoanode, and Co<sub>3</sub>O<sub>4</sub>/ZnGaNO microrod photoanode in dark and under AM 1.5G-simulated sunlight.

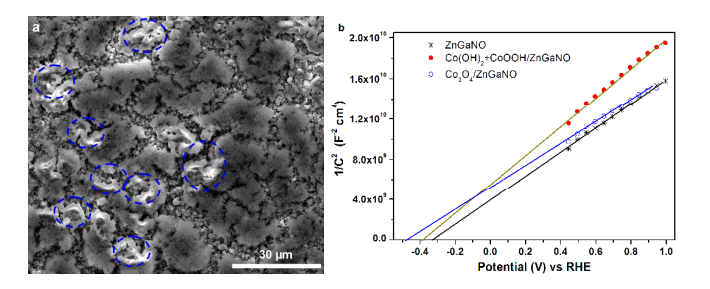


**Fig. 4** a) SEM image for the mixture of Co(OH)<sub>2</sub> and CoOOH loaded porous ZnGaNO microrod photoelectrode. Blue circles indicate the interface between Cobased catalyst and ZnGaNO exposed by a high pressure gas purging. b) The Mott-Schottky plots for ZnGaNO, Co(OH)<sub>2</sub>+CoOOH/ZnGaNO and Co<sub>3</sub>O<sub>4</sub>/ZnGaNO were measured by performing a potential scan in the anodic direction under a frequency of 1 kHz and an AC amplitude of 10 mV in 1M NaOH.

The enhancing effect of Co-containing electrocatalysts on photoelectrochemical activity of the ZnGaNO microrod photoanode is ascribed to the improved surface properties of the microrod for water splitting. Mott-Schottky analysis (**Fig. 4b**) showed that the flatband potential of the surface modified ZnGaNO shifted cathodically by 80mV for as-prepared Co-based electrocatalyst and 150mV for Co<sub>3</sub>O<sub>4</sub> relative to that of the unloaded ZnGaNO. Noting that flat-band potential for the modified and unmodified ZnGaNO was -0.3~-0.5 V vs. RHE, which usually corresponds to the photocurrent onset potential. However, an obvious anodic photocurrent was observed at about bias 0.2V vs. RHE. Usually, the photocurrent onset potential is mainly affected by electron-hole recombination and slow reaction kinetics of holes

semiconductor. In our case, the Co-based electrocatalyst was used to improve the oxygen-evolving kinetics and suppress the electron-hole recombination. When the bias higher than 0.2V, a cathodic current was observed on the bare ZnGaNO with cocatalyst modification (Fig. S12 see ESI†), which can be attributed to the back reaction such as O<sub>2</sub> reduction. Indeed, increasing the loading content of the Co-based catalyst will suppress the back reaction due to the dense catalyst layer coating on the ZnGaNO surface (Fig.S13,see ESI†). The cathodic photocurrent started at about -0.3V, close to the flat-band potential. The observed photocurrent was decreased when increasing the loading content of the Co-based catalyst due to the decrease in light absorption by Co-containing species. Coating the passivating layer on the ZnGaNO surface probably is the good choice for suppressing the back reaction. The cathodic shift of the flatband potential indicated the strong interaction between Co-containing electrocatalysts and ZnGaNO. Compared to the Co<sub>3</sub>O<sub>4</sub>, the asprepared Co-based electrocatalyst modification showed the slightly weak effect on cathodic shift of the flatband potential of ZnGaNO. However, the as-prepared Co-based electrocatalyst loading induces a significant enhancement in photoelectrochemical activity of ZnGaNO, further demonstrating that the as-prepared Co-based electrocatalyst has excellent electrocatalytic performance for water splitting, as confirmed by cyclic voltammetry analysis.

#### 4. Conclusions

To summarize, a new route for preparing the ZnGaNO porous microrods is reported here. The reaction pathway involves a ZnO single crystal internal decomposition process in the microrod via the nitriding reaction with KGaO2. The morphology of ZnO precursor can be inherited by ZnGaNO, meaning that nitriding the different morphologies of ZnO will obtain the porous ZnGaNO with various morphologies. The proposed synthetic strategy extends the possibility of porous microstructure building to a range of functional ceramics and semiconductors. A predictable example is that the porous Zn<sub>1+x</sub>GeN<sub>2</sub>O<sub>x</sub> microrods can be synthesized by nitriding the Na<sub>2</sub>GeO<sub>3</sub> colloid coated ZnO microrods via a similar single crystal internal decomposition route. Therefore, the proposed single crystal internal decomposition route extends the possibility of porous structure constructing of oxynitrides to a range of functional ceramics and semiconductors. The ZnGaNO porous microrods exhibited the high performance in the photoelectrochemical water splitting due to the low defects density, the increasing electrolyte contact area by porous structure and the shorting charge carrier transfer distance by nanocrystal. A new electrocatalyst, the mixed Co-based oxides of Co(OH)<sub>2</sub> and CoOOH, was developed to further increase the photoelectrochemical performance of ZnGaNO.

#### Acknowledgments

This work is supported by the National Basic Research Program of China (973 Program, 2013CB632404), the National Natural Science Foundation of China (Nos. 51102132, 11174129, 51272101, and 51272102) and the State Key Laboratory of NBC Protection for Civilian. (No.SKLNBC2014-09)

#### Notes and references

<sup>a</sup> Collaborative Innovation Center of Advanced Microstructures, Nanjing University, NO. 22, Hankou Road, Nanjing, Jiangsu 210093, P.R.China
 <sup>b</sup> Eco-Materials and Renewable Energy Research Center (ERERC), College of Engineering and Applied Sciences, Nanjing University, NO. 22, Hankou Road, Nanjing, Jiangsu 210093, P.R.China, E-mail: yscfei@nju.edu.cn

<sup>c</sup> National Laboratory of Solid State Microstructures, School of Physics, Nanjing University, NO. 22, Hankou Road, Nanjing, Jiangsu 210093, P.R.China

†Electronic Supplementary Information (ESI) available: Details of experimental procedures, characterizations, and supporting images.See DOI: 10.1039/c000000x/

- 1 D.L. Lu, T. Takata, N. Saito, Y. Inoue and K. Domen, Nature 2006, 440,
- 295. 2 W.T. Chen, H.S. Sheu, R.S.Liu and J. P. Attfield. *J. Am. Chem. Soc.*, 2012, **134**, 8022.
- 3 D. Oka, Y. Hirose, H. Kamisaka, T. Fukumura, K. Sasa,S. Ishii, H.Matsuzaki, Y. Sato, Y. Ikuhara and T. Hasegawa. *Sci. Rep.* 2014, **4**, 4987 4 M. Jansen and H. P. Letschert, *Nature* 2000, **404**, 980.
- 5 H. Tong, S. X. Ouyang, Y. P. Bi, N. Umezawa, M. Oshikiri and J. H. Ye, *Adv. Mater.* 2012, **24**, 229.
- 6 F. E. Osterloh. Chem. Soc. Rev., 2013, 42, 2294.

**Journal Name** 

- 7 H. G. Yang, C. H. Sun, S. Z. Qiao, J. Zou, G. Liu, S. C. Smith, H. M. Cheng and G. Q. Lu, *Nature* 2008, **453**, 638. 8 S. C. Yan, S X. Ouyang, J. Gao, M. Yang, J. Y. Feng, X. X. Fan, L. J. Wan,
- Z. S. Li, J. H. Ye, Y. Zhou and Z.G. Zou, Angew. Chem. Int. Ed., 2010, 49, 6400.
- 9 K.Sivula, F. L.Formal and M. Grätzel. ChemSusChem. 2011, 4, 432.
- 10 S. C. Warren, K. Voïtchovsky, H. Dotan, C. M. Leroy, M. Cornuz, F. Stellacci, C. Hébert, A. Rothschild and Michael Grätzel. Nature Mater. 2013,
- 11 W.J. Luo , Z.S. Yang , Z.S.Li, J.Y. Zhang , J.G. Liu , Z.Y. Zhao , Z.Q.Wang , S.C.Yan, T.Yu and Z.G. Zou, *Energy Environ. Sci.*, 2011, 4,
- 12 T.W. Kim and K. S. Choi, Science, 2014, 343, 990.
- 13 J. Haskouri, S. Cabrera, F. Sapiña, J. Latorre, C. Guillem, A. Beltrán-Porter, D. Beltrán-Porter, M. Dolores Marcos and P. Amorós, *Adv. Mater.* 2001, 13, 192.
- 14 I. Nowak and M. Ziolek, Catal. Today 2006, 118, 410.
- 15 S.C. Yan, Z.Q. Wang, Z.S. Li and Z.G. Zou. *J. Mater. Chem.* 2011, **21**, 5682. 16 S.C. Yan, H. Yu, N.Y. Wang, Z.S. Li and Z.G. Zou. *Chem. Communi.* 2012, **48**, 1048.
- 17 D.L. Lu, G. Hitoki, E. Katou, J. N. Kondo, M. Hara and K. Domen, Chem.
- Mater. 2004, 16, 1603.

  18 J.Y.Feng, W.J.Luo, T.Fang, H.Lv, Z.Q.Wang, J.Gao, W.M.Liu, T.Yu, Z.S.Li and Z.G.Zou, Adv. Funct. Mater. 2014, 24, 3535.

  19 H.Suhulz and K. H.Thiemann, Solid State Commun. 1977, 23, 815.
- 20 O.Garcia-Martinez, R. M.Rojas, E.Vila and J. L.Martin de Vidales, Solid State Ionics 1997, **63**, 442.
- 21 L. Jensen, J. T. Muckerman and M. D. Newton, *J. Phys. Chem. C*, 2008, **112**, 3439.
- 22 H. Hashiguchi, K. Maeda, R. Abe, A. Ishikawa, J.Kubota and K. Domen. *Bull. Chem. Soc. Jpn.* 2009, **82**, 401.
  23 A. B. Djurišić, Y. H. Leung, K. H. Tam, L. Ding, W. K. Ge, H. Y. Chen and S. Gwo. *Appl. Phys. Lett.* 2006, **88**, 103107.

- 24 D. Li, Y. H. Leung, A. B. Djurišić, Z. T. Liu, M. H. Xie, S. L. Shi, S. J. Xu and W. K. Chan. *Appl. Phys. Lett.*, 2004, **85**, 1601.
  25 E. J. W. Crossland, N. Noel, V. Sivaram, T. Leijtens, J. A. Alexander-Webber and H. J. Snaith. *Nature* 2013, **495**, 215.
- 26 M. W. Kanan, Y. Surendranath and D. G. Nocera, Chem. Soc. Rev., 2009, **38**, 109.
- 27 M.E.G Lyons and M.P Brandon. Int.J. Electrochem.Sci., 2008, 3, 1425.
- M. W. Kanan and D. G. Nocera. *Science* 2008, **321**, 1072.
   M.J. Liao , J.Y. Feng , W.J. Luo , Z.Q. Wang , J.Y. Zhang , Z.S. Li , T.Yu and Z.G.Zou. *Adv. Funct. Mater.* 2012, **22**, 3066.
   K. Maeda, K. Teramura, N. Saito, Y. Inoue and K. Domen. *J. Catal.* 2006,
- **243**, 303.